THESIS FOR THE DEGREE OF LICENTIATE OF ENGINEERING

Dilute Cu-Pd Alloys for Practical CO_2 Electroreduction

Arma Yau Musa

Department of Chemistry and Chemical Engineering

CHALMERS UNIVERSITY OF TECHNOLOGY

Gothenburg, Sweden 2026

Dilute Cu-Pd Alloys for Practical CO_2 Electroreduction
ARMA YAU MUSA

Licentiatuppsatser vid Institutionen för kemi och kemiteknik
Chalmers tekniska högskola
Nr 2026:12

Department of Chemistry and Chemical Engineering
Chalmers University of Technology
SE-412 96 Gothenburg
Sweden
Telephone + 46 (0)31-772 1000

Chalmers Digitaltryck
Gothenburg, Sweden 2026

Dilute Cu-Pd Alloys for Practical CO_2 Electroreduction

ARMA YAU MUSA

Department of Chemistry and Chemical Engineering
Chalmers University of Technology

Abstract

Electrochemical conversion of CO_2 into fuels and value-added chemicals offers a compelling route to simultaneously address fossil fuel dependence and renewable energy intermittency. Copper is the only monometallic electrocatalyst capable of reducing CO_2 to multi-carbon (C_{2+}) products such as ethylene and ethanol, making it the central focus of efforts to develop practical CO_2 electrolysis technologies. However, two fundamental challenges limit progress: the difficulty of achieving and maintaining high C_{2+} selectivity on Cu-based catalysts, and the lack of in-depth studies conducted under industrially relevant operating conditions at high current densities. Dilute alloying, which is the incorporation of trace amounts of a secondary metal into the Cu host lattice, has emerged as a promising strategy to modify Cu surface reactivity and its C-C coupling capability. Yet, the influence of preparation method on the atomic-scale structure of dilute alloy nanoparticles, and how that structure governs electrocatalytic performance, remains poorly understood. In this thesis, the effect of Cu-Pd dilute alloy composition and synthesis route was investigated. It was shown that they jointly govern the structure and CO_2 electroreduction performance of Cu-Pd dilute alloy nanoparticles in zero-gap electrolyzers at industrially relevant current densities. Cu-Pd dilute alloy nanoparticles with controlled Pd compositions were prepared by two wet-chemical routes; sequential reduction and co-reduction, and tested at high current densities in zero-gap electrolyzers.

The results demonstrate that dilute Pd alloying functions as a stability promoter under high-rate operating conditions, suppressing the current-density-dependent surge in hydrogen evolution that afflicts pure Cu and preserving faradaic efficiency toward CO_2 reduction products. Furthermore, sequential reduction may preferentially produce Cu-Pd alloys with isolated surface Pd sites which outperform Cu-Pd alloys prepared via co-reduction at equivalent bulk composition. Together, these findings demonstrate that composition and synthesis routes must be jointly optimized to provide transferable design principles for robust and selective Cu-based electrocatalysts for practical CO_2 electroreduction systems.

Keywords: CO_2 electroreduction, dilute alloy catalysts, multicarbon selectivity, zero-gap electrolyzer, synthesis route, catalyst stability

List of Publications

This thesis is based on the following appended papers:

Paper I:

Dilute Pd Alloying as a Stability Promoter for Cu-Based CO_2 Electroreduction Catalysts in Zero-Gap Electrolysers

Arma Yau Musa, Mohd Monis Ayyub, Michael Wilms, Andrew Yankovich, Lunjie Zeng, Brian Seger and Mathilde Luneau*

Manuscript

Paper II:

Sequential Reduction vs Coreduction: Controlling Structure and Performance of Cu-Pd Dilute Alloy Catalysts

Arma Yau Musa, Mohd Monis Ayyub, Michael Wilms, Andrew Yankovich, Lunjie Zeng, Brian Seger and Mathilde Luneau*

Manuscript

My Contribution

Paper I:

I synthesized all the samples, performed the electrochemical tests and collected the TEM images. I interpreted the results and wrote the first draft of the manuscript, which was iterated and finalized together with my co-authors.

Paper II:

I synthesized all the samples, performed the electrochemical tests and collected the TEM images. I interpreted the results and wrote the first draft of the manuscript, which was iterated and finalized together with my co-authors.

Other publications

The following manuscript has been submitted during my studies but is not included in the thesis.

Highly Ordered Pd/CeO_x Inverse Opals for Alkaline Hydrogen Oxidation

Michael Wilms, Arma Yau Musa, Ruby Susan Raju, Deya Sallaberry, and Mathilde Luneau*

Nanoscale (2026), doi: 10.1039/d6nr00422a

Abbreviations

*CO	Adsorbed carbon monoxide
*COOH	Adsorbed carboxyl intermediate
*H	Adsorbed hydrogen
AA	Ascorbic acid
AEM	Anion exchange membrane
Au	Gold
Ag	Silver
C_1	Single carbon products
C_{2+}	Multi-carbon products
CO_2RR	CO_2 electroreduction reaction
Cu	Copper
CuOAc	Copper(I) acetate
CuPd	Copper-palladium alloy
DFT	Density functional theory
EDS	Energy-dispersive X-Ray spectroscopy
FE	Faradaic efficiency
GC	Gas chromatography
GDE	Gas diffusion electrode
GDL	Gas diffusion layer
HAADF-STEM	High-angle annular dark-field scanning transmission electron microscopy

HER	Hydrogen evolution reaction
HPLC	High-performance liquid chromatography
ICP-MS	Inductively coupled plasma mass spectrometry
Ir	Iridium
MEA	Membrane electrode assembly
MPL	Microporous layer
NMR	Nuclear magnetic resonance
NPs	Nanoparticles
OER	Oxygen evolution reaction
Pd	Palladium
$Pd(OAc)_2$	Palladium(II) acetate
Pt	Platinum
RHE	Reversible hydrogen electrode
SAA	Single atom alloy
SEM	Scanning electron microscopy
SHE	Standard hydrogen electrode
STEM-EDS	Scanning transmission electron microscopy with energy-dispersive X-ray spectroscopy
TCD	Thermal conductivity detector
TDPA	Tetradecylphosphonic acid
TEM	Transmission electron microscopy
TOA	Trioctylamine

XPS	X-Ray photoelectron spectroscopy
XRD	X-ray diffraction

Table of Contents

1. Introduction

Electrochemical CO_2 reduction research is motivated by the urgent need to reduce dependence on fossil fuels and mitigate greenhouse gas emissions. Global energy demand continues to rise as societies strive to maintain and improve living standards. Presently, much of this demand is met through the combustion of fossil fuels, resulting in a steady increase in atmospheric carbon dioxide and other greenhouse gases. Consequently, global weather patterns are already undergoing measurable changes, with increasingly severe environmental and societal impacts predicted for the future.[1]

Although modern economies and lifestyles are deeply dependent on fossil fuels, there are compelling reasons to transition toward alternative energy sources and carbon feedstocks. Beyond climate change, fossil fuel extraction and utilization contribute significantly to air[2,3] and water pollution,[4] resulting in adverse impacts on human health and substantial economic costs. Fossil fuel dependence has also been associated with broader socio-economic challenges, including geopolitical instability and resource-driven conflicts.[5]

Despite these concerns, the transition away from fossil fuels has been hindered by economic constraints and the limited availability of scalable alternatives. However, the rapidly decreasing cost of renewable energy technologies, combined with growing awareness of the environmental and societal consequences of fossil fuel use, is creating new opportunities for change. Among renewable energy sources, wind[6] and solar[7] offer the largest untapped potential and are theoretically sufficient to meet global electricity demand. Nevertheless, their intermittent nature presents a fundamental challenge to large-scale grid integration, as variability in supply can lead to grid instability and power fluctuations.

To enable higher penetration of renewable electricity, efficient and scalable energy storage technologies are required to store excess energy during periods of high generation and release it when demand exceeds supply. At present, no existing energy storage technology can fully meet this challenge at the necessary scale and cost. In parallel, the transition away from fossil fuels also requires alternative carbon sources to produce fuels and chemicals. While biomass represents a potential renewable carbon feedstock, its large-scale deployment is constrained by competition with land for food production and conservation, as well as associated environmental and human health concerns.[8]

Electrochemical conversion of CO_2 into fuels and value-added chemicals offers a compelling alternative to address the challenges associated with fossil fuel dependence and renewable

energy intermittency. By utilizing CO_2 as a carbon source, this approach enables the direct coupling of renewable electricity to chemical energy storage while supporting sustainable fuel and chemical production. In this way, CO_2 electroreduction provides a pathway to close the carbon cycle by converting emitted CO_2 into fuels and chemicals using renewable electricity, forming an artificial carbon cycle (Figure 1.1).[9]

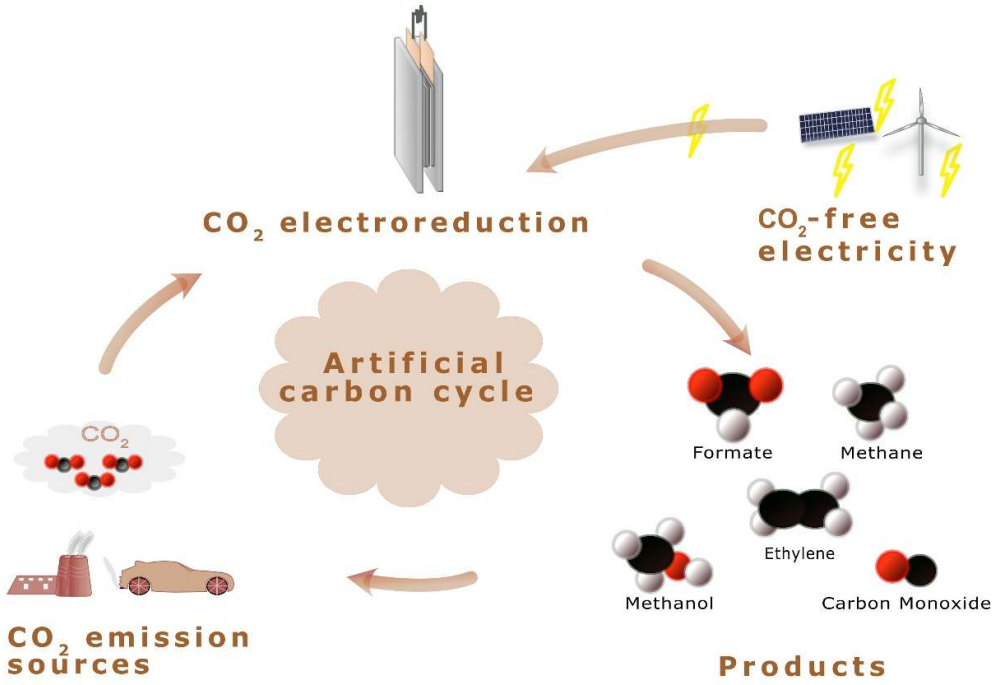

Figure 1.1: CO_2 recycling via artificial carbon cycle.

Copper (Cu) is one of the most promising electrocatalysts for the electrochemical reduction of CO_2 to value-added multicarbon (C_{2+}) chemicals and fuels. However, the development of practical CO_2 electroreduction technologies remains limited by two major challenges: the difficulty of achieving high selectivity toward C_{2+} products on Cu-based catalysts, and the lack of in-depth studies conducted under industrially relevant operating conditions, particularly at high current densities. While dilute alloying (where trace amounts of a secondary metal are incorporated into a primary metal matrix) has emerged as a promising strategy to tune surface electronic structure and reaction intermediates,[10] this class of materials remains underexplored for CO_2 electroreduction, especially with respect to how synthesis and preparation routes influence catalytic behavior.

The objective of this thesis is to establish how alloy composition and synthesis pathway jointly govern the structural stability and electrocatalytic selectivity of Cu-based dilute alloy

The objective of this thesis is to establish how alloy composition and synthesis pathway jointly govern the structural stability and electrocatalytic selectivity of Cu-based dilute alloy nanoparticles for CO_2 electroreduction toward multi-carbon products. Using Cu-Pd dilute alloys as a model system, this work investigates how controlled variations in Pd content and preparation method influence nanoparticle structure, resistance to electrochemical restructuring and compositional change, and performance retention in zero-gap membrane electrode assembly electrolysers operating at high current densities. Central to this investigation is understanding how the atomic dispersion of Pd within the Cu host modifies the electronic environment of Cu active surface sites and how this modification stabilizes C-C coupling intermediates to sustain selective C_{2+} production under prolonged operation. The insights gained are intended to provide further understanding into design principles for robust, selective, and scalable Cu-based electrocatalysts for practical CO_2 electroreduction systems.

2. Background

2.1 Electrochemistry

Electrochemistry is concerned with the relationship between electrical energy and chemical reactions. It involves the study of how spontaneous chemical reactions can be exploited to generate electricity, and conversely, how an applied electrical potential can be used to drive non-spontaneous reactions.[11]

The history of electrochemistry spans several centuries, from the earliest observations of electricity-induced chemical change in the late 18th century, to the sophisticated electrochemical systems of today including batteries, fuel cells, and electrolysers. The concepts most relevant to this thesis concern redox reactions and their behavior under applied potentials, the thermodynamics governing electrochemical systems, and the sources of inefficiency that must be minimized in practical devices.[12]

Redox reactions are a class of chemical reactions in which electrons are transferred between species, causing changes in their oxidation states.[13] The term derives from reduction and oxidation, the two complementary half-reactions of gaining and losing electrons, respectively, represented by the general reaction:

$$\mathrm{X} + \mathrm{Y} \rightarrow \mathrm{X}^{n+} + \mathrm{Y}^{n-}$$

Here, X is oxidized by donating *n* electrons, while Y is reduced by accepting them. Any redox reaction can be decomposed into two half-reactions:

$$\mathrm{X} \rightarrow \mathrm{X}^{n+} + ne^{-} \quad \text{(oxidation)}$$
$$\mathrm{Y} + ne^{-} \rightarrow \mathrm{Y}^{n-} \quad \text{(reduction)}$$

A key feature of electrochemical systems is that these two half-reactions, while always occurring simultaneously, can be physically separated in space. This separation is the fundamental basis for all practical electrochemical devices.[14]

2.2 Electrochemical systems

A typical electrochemical cell consists of two electrodes; an anode and a cathode, connected by both an external electric circuit and the electrolyte that conducts ions between them (Figure 2.1). Oxidation occurs at the anode where electrons are released into the external circuit, while electrons are consumed at the cathode via reduction. The resulting flow of electrons leads to a measurable electric current. Simultaneously, ions generated at one electrode migrate through the electrolyte toward the opposite electrode to maintain overall charge neutrality within the cell.

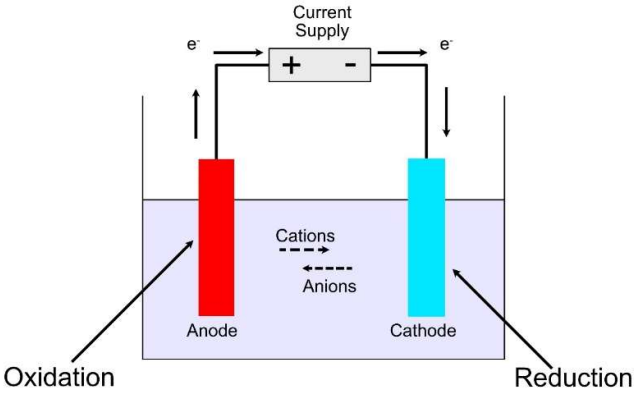

Figure 2.1: Schematic of an Electrochemical cell.

Each electrode is characterized by its standard reduction potential which is how readily the associated half-reaction proceeds in the reductive direction. Reduction potentials are defined relative to the standard hydrogen electrode (SHE), for which the reaction:

$$\frac{1}{2}\mathrm{H_2} \rightleftharpoons \mathrm{H^+} + \mathrm{e^-} \tag{2.1}$$

is assigned a potential of 0 V under standard conditions.

The total cell potential is defined by convention as the difference between the cathode and anode reduction potential:

$$E_{\mathrm{cell}} = E_{\mathrm{cathode}} - E_{\mathrm{anode}} \tag{2.2}$$

This quantity determines both the spontaneity of the reaction (E > 0) and the maximum electrical work W_{max} obtainable from the system:

$$W_{\mathrm{max}} = -n\mathrm{F}E_{\mathrm{cell}} \tag{2.3}$$

where n is the number of electrons transferred and F = 96485 $Cmol^{-1}$ is the Faraday constant.[14,15]

2.3 Thermodynamics of electrochemical reactions

The Gibbs free energy ΔG determines the thermodynamic driving force for any electrochemical reaction.[12] For a spontaneous electrochemical reaction such as in a fuel cell, $\Delta G < 0$; while for a non-spontaneous reaction such as in water splitting and CO_2 electroreduction, $\Delta G > 0$. The relationship between $\Delta G$and the cell potential is:

$$\Delta G = -n\mathrm{F}E_{\mathrm{cell}} \tag{2.4}$$

The dependence of the cell potential on reactant and product concentrations is described by the Nernst equation, derived from the standard thermodynamic expression $\Delta G = \Delta G^0 + \mathrm{R}T\ln\ Q_\mathrm{r}$[12]:

$$E_{\text{cell}} = E^0_{\text{cell}} - \frac{\mathrm{R}T}{nF}\ln Q_r \qquad (2.5)$$

where E^0_{cell} is the standard cell potential, R is the gas constant, T is temperature, and Q_r is the reaction quotient. The Nernst equation is particularly important in CO_2 electroreduction, as the equilibrium potentials of the various possible reduction products are concentration dependent, and operating conditions such as local pH and CO_2 partial pressure directly influence the thermodynamic landscape of the reaction.[16]

2.4 Overpotential losses

The conversion efficiency of any practical electrochemical system is always less than unity. The overpotential η represents the difference between the actual operating potential E_{cell} and the thermodynamic equilibrium potential E^0_{cell} given by:

$$\eta = E_{\text{cell}} - E^{\text{o}}_{\text{cell}} \qquad (2.6)$$

The differenc arises from several distinct sources of loss, which are important to understand both for fundamental electrochemical systems and for the practical deployment of CO_2 electrolysers.

2.4.1 Activation losses

Activation losses originate from the activation energy barriers that must be overcome for electrode reactions to occur at a finite rate.[15] Even with a catalyst, some barrier remains, and its magnitude is highly reaction dependent. The relationship between current (i.e. reaction rate) and activation overpotential is described by the Butler-Volmer equation:[17]

$$i = i_0\left(e^{\frac{(1-\alpha)n\mathrm{F}\eta}{\mathrm{R}T}} - e^{\frac{-\alpha n\mathrm{F}\eta}{\mathrm{R}T}}\right) \qquad (2.7)$$

where i_o is the exchange current density at equilibrium and α is the charge transfer coefficient that describes the symmetry of the energy barrier with respect to the applied potential. At large overpotentials, this expression simplifies to the Tafel equation:[17]

$$\eta = \mathrm{a} + \mathrm{b}.\log(i) \qquad (2.8)$$

where b is the Tafel slope, a parameter that widely determines the reaction mechanisms (Figure 2.2).

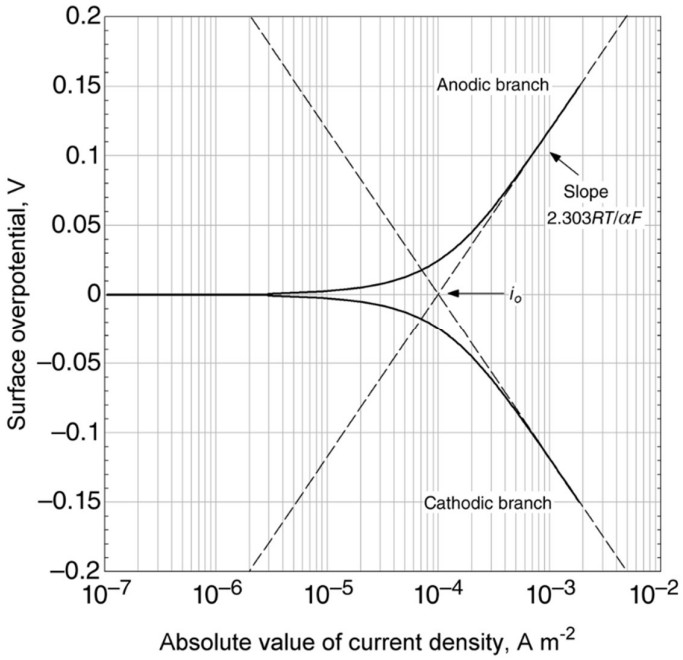

Figure 2.2: Classic Tafel plot. Taken from reference [18]

2.4.2 Ohmic losses

Ohmic losses arise from resistance to electron flow in electrode materials and external connections, as well as resistance to ion transport in the electrolyte and membrane. These losses scale linearly with current and become increasingly significant at higher current densities, placing demands on cell design and electrolyte/membrane conductivity.[12,15]

2.4.3 Mass transport losses

Mass transport losses occur when the rate of reactant supply to the electrode surface is insufficient to sustain the electrochemical reaction. In CO_2 electroreduction, this is a particularly important consideration, as CO_2 has limited solubility in aqueous electrolytes (33 mM at room temperature and atmospheric pressure).[19] At high current densities, CO_2 is depleted near the electrode surface faster than it can be replenished by diffusion, leading to a drop in local concentration, a shift in local pH, and ultimately a reduction in selectivity toward CO_2 reduction products relative to the competing hydrogen evolution reaction (HER).[20] Gas diffusion electrodes and flow cell architectures have been developed specifically to mitigate these mass transport limitations by supplying CO_2 directly to the catalyst surface in the gas phase.[21]

2.5 Catalysis and electrocatalysis

Electrochemical reactions are controlled by both thermodynamics and kinetics. Thermodynamics indicates whether a reaction is energetically favorable, whereas kinetics determines how quickly the reaction occurs in practice. Even if a reaction is thermodynamically spontaneous, it still requires overcoming the activation energy barrier before products can be formed. This is why catalysis plays a crucial role.

A catalyst enhances the kinetic rate of a chemical reaction by offering an alternative pathway with a lower activation energy, while remaining unchanged at the end of the process (Figure 2.3). Three key principles define catalytic behavior:[22]

1. A catalyst reduces the activation energy by enabling a reaction pathway with a lower energy barrier, allowing the reaction to proceed more rapidly under the same conditions.
2. While the activation energy is lowered, the overall thermodynamics of the reaction remain unaffected. The Gibbs free energy difference between reactants and products does not change, meaning the catalyst does not alter the equilibrium position. Instead, it influences only the reaction rate, accelerating both the forward and reverse reactions equally.
3. A catalyst provides specific surface sites where reactants can adsorb, interact, and come into proximity, effectively facilitating their interaction and promoting the reaction.

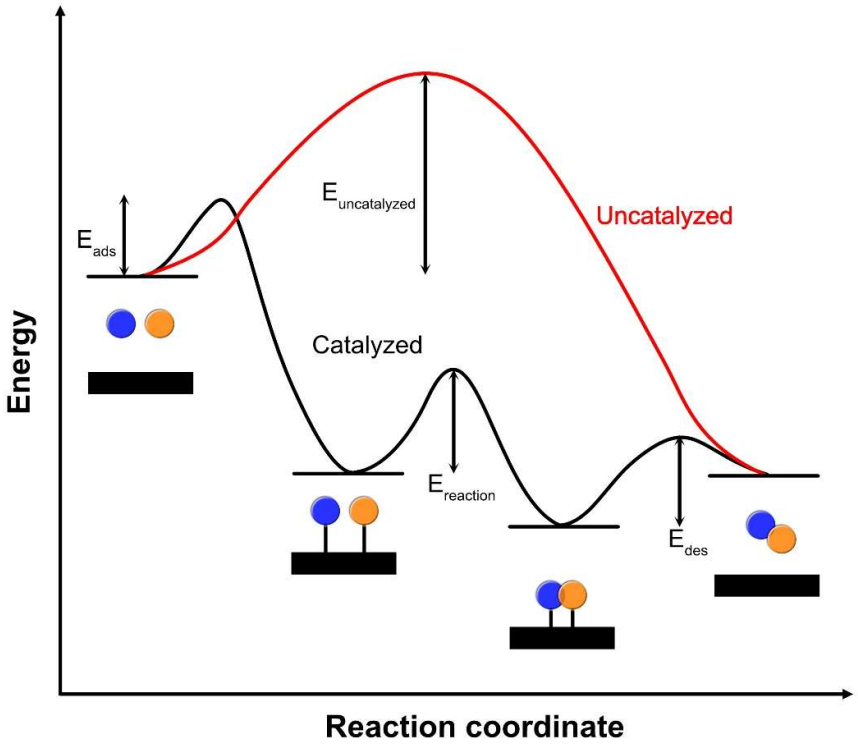

Figure 2.3: Energy diagram showing how a catalyst lowers the activation barrier of a chemical reaction relative to the uncatalyzed pathway.

The requirements for an effective catalyst are described by the Sabatier principle, which states that reactants should bind to the catalyst surface with neither too strong nor too weak an affinity.[23] If the interaction is too weak, reactants cannot properly adsorb or activate on the surface. Conversely, if the binding is too strong, reaction intermediates remain attached and block active sites, limiting further turnover. This means that every catalytic system has an optimal binding strength, and identifying materials that approach this optimum is a key goal in catalyst design. Catalysts drive selectivity by preferentially stabilizing the transition state of a desired reaction pathway over competing ones, through geometric constraints, electronic effects, and non-covalent interactions at the active site. Even small energy differences between transition states translate into large selectivity outcomes.

Electrocatalysis follows these same fundamental ideas, with one crucial addition: the applied electrode potential provides a direct way to control reaction rates and product selectivity by tuning the energy of electrons at the catalyst surface. In this context, electrocatalyst performance is defined by three main parameters:

(1) activity, which describes how fast the desired reaction occurs – commonly expressed as a current density (mA cm^{-2}).
(2) selectivity, which reflects the preference for forming a specific product over competing ones – commonly expressed a faradaic efficiency is the fraction of total electrical charge passed in an electrochemical reaction that contributes to the desired product, expressed as a percentage.
(3) stability, which refers to the ability to sustain performance over time under electrochemical conditions.[24]

2.6 Electrochemical CO_2 reduction reaction (CO_2RR)

The extensive use of fossil fuels has led to an increase in atmospheric CO_2 concentrations, which is widely recognized as a primary driver of global climate change.[25] One promising strategy to mitigate CO_2 emissions is the CO_2 electroreduction into value-added chemicals and fuels. This approach has attracted considerable interest because it has the potential to simultaneously provide pathway to sustainable energy storage and chemical synthesis, particularly when coupled with renewable electricity sources.[26] Moreover, CO_2RR can be conducted under relatively mild conditions and offers tunable selectivity toward a range of products, making it an attractive technology for the chemical industry.

CO_2RR is an electrolytic process in which an externally applied potential drives the reduction of CO_2 at the cathode, while the oxygen evolution reaction (OER) typically proceeds at the anode. However, it is intrinsically challenging due to the molecule's high thermodynamic stability, linear geometry, and nonpolar nature. As a result, significant energy input is required to activate CO_2 and drive its transformation into reduced products. Furthermore, CO_2 electroreduction involves multiple proton- and electron-transfer steps, which can lead to a wide range of products depending on reaction conditions and catalyst properties. Consequently, the performance of the CO_2 electroreduction is strongly governed by the catalyst's ability to adsorb and activate CO_2, stabilize key reaction intermediates, and maintain structural and chemical stability under operating conditions.[27,28]

2.6.1 Standard reduction potentials

From the thermodynamic principle established in the previous section, it is imperative to consider the standard reduction potential of various reaction pathways in CO_2RR. CO_2RR can yield a diverse set of products due to the different numbers of electrons and protons involved. Typical products are CO, CH_4, C_2H_4, and C_2H_5OH. The standard reduction potentials for CO_2

reduction to various products at room temperature, atmospheric pressure, and pH 7 (vs. SHE) are summarized below:[29,30]

$CO_2 + 2H^+ + 2e^- \longrightarrow CO + H_2O$ $E^o = -0.52$ V (2.9)

$CO_2 + 4H^+ + 2e^- \longrightarrow HCHO + H_2O$ $E^o = -0.51$ V (2.10)

$CO_2 + 2H^+ + 2e^- \longrightarrow HCOOH + H_2O$ $E^o = -0.61$ V (2.11)

$CO_2 + 8H^+ + 8e^- \longrightarrow CH_4 + 2H_2O$ $E^o = -0.24$ V (2.12)

$2CO_2 + 12H^+ + 12e^- \longrightarrow C_2H_4 + 4H_2O$ $E^o = -0.34$ V (2.13)

$CO_2 + 6H^+ + 6e^- \longrightarrow CH_3OH + H_2O$ $E^o = -0.38$ V (2.14)

$CO_2 + 12H^+ + 12e^- \longrightarrow CH_3CH_2OH + H_2O$ $E^o = -0.33$ V (2.15)

$2H^+ + 2e^- \longrightarrow H_2$ $E^o = -0.42$ V (2.16)

$CO_2 + e^- \longrightarrow CO_2^{\bullet -}$ $E^o = -1.90$ V (2.17)

From these values, it is apparent that direct CO_2 electroreduction via a one-electron transfer to form the CO_2 anion radical ($CO_2^{\bullet -}$) is highly unfavorable, with a formal reduction potential of approximately −1.90 V versus SHE, in aqueous media at pH 7. This high energetic cost of CO_2 activation and the unfavorable thermodynamics of direct electroreduction highlight that an effective electrocatalyst for CO_2 electroreduction should operate at low overpotential while delivering high activity and selectivity toward the desired products, in addition to maintaining structural and compositional stability under operating conditions. As a result, catalytic strategies such as careful design of catalyst composition, structure, and local reaction environment that modify the local reaction environment and stabilize key reaction intermediates typically become the primary motive. The aim is to bypass the formation of $CO_2^{\bullet -}$ by promoting proton-assisted, multi-electron transfer pathways, thereby enabling efficient CO_2 electroreduction at significantly lower energetic cost. Also, another fundamental challenge in CO_2 electroreduction is the competition between CO_2 electroreduction and the hydrogen evolution reaction (HER), in which protons from the aqueous electrolyte are reduced to molecular hydrogen at the cathode (represented in equation 2.16). Since HER and CO_2 electroreduction occur simultaneously at the cathode under similar potential windows, suppressing hydrogen evolution while maintaining high CO_2RR selectivity is one of the central challenges in catalyst design.

2.6.2 Cell configurations

In practice, CO_2 electroreduction is typically carried out in an electrochemical cell comprising a cathode compartment (where CO_2 electroreduction happens), an anode compartment (where OER happens), and an ion-exchange membrane separating the two compartments. The

membrane enables ionic charge transport while preventing electronic short-circuiting and suppressing re-oxidation of reduced CO_2 products at the anode. The electrochemical cell majorly comes in 3 different configurations (Figure 2.4), each offering distinct benefits and limitations:[31]

1. The H-cell configuration is widely used for fundamental CO_2 electroreduction studies (Figure 2.4a). In this setup, the cathodic compartment is filled with a CO_2-saturated bicarbonate electrolyte, which is continuously bubbled with CO_2 to maintain CO_2 saturation and enable quantification of gaseous products, while liquid products are typically analyzed post-reaction using techniques such as NMR or HPLC. Despite its simplicity and widespread adoption, the H-cell suffers from limited CO_2 availability at the cathode surface due to the low solubility of CO_2 in aqueous electrolytes. These mass transport limitations lead to low current densities (< 10 mA cm^{-2}) and favor the competing hydrogen evolution reaction.
2. Liquid flow-cells have emerged as a compelling alternative to conventional H-cells by effectively overcoming mass-transport limitations (Figure 2.4b). In these systems, a catalyst layer is deposited onto a porous gas diffusion layer that serves as the cathode, enabling direct delivery of gaseous CO_2 to a stable gas-liquid-solid interface and allowing operation at current densities exceeding 100 mA cm^{-2}. Beyond enhanced reactant transport, flow cells enable operation in highly alkaline electrolytes, which suppress the hydrogen evolution reaction and promote C-C coupling through a locally alkaline reaction environment. However, large-scale implementation remains challenged by ohmic losses, electrode flooding, carbonate formation, and salt accumulation, highlighting the need for continued advances in energy efficiency, electrolyte management, CO_2 utilization, and long-term operational stability.
3. Zero-gap electrolyzers based on a membrane electrode assembly (MEA) improve on flow cells by offering reduced cell resistance, high current densities, and improved energy efficiency (Figure 2.4c). Here, the membrane is sandwiched between cathodic and anodic gas diffusion electrodes, enabling intimate catalyst-membrane contact while eliminating the need for a bulk liquid catholyte. This zero-gap architecture retains the advantages of gas diffusion electrode-based designs while minimizing electrolyte consumption and enabling compact, scalable operation, with recent demonstrations achieving high faradaic efficiencies and industrially relevant current densities. Despite these advantages, large-scale deployment is hindered by challenges including carbonate

crossover, cathode flooding, catalyst and membrane degradation, water and ion management issues, and trade-offs between ionic conductivity and proton availability under high-current, alkaline operating conditions.

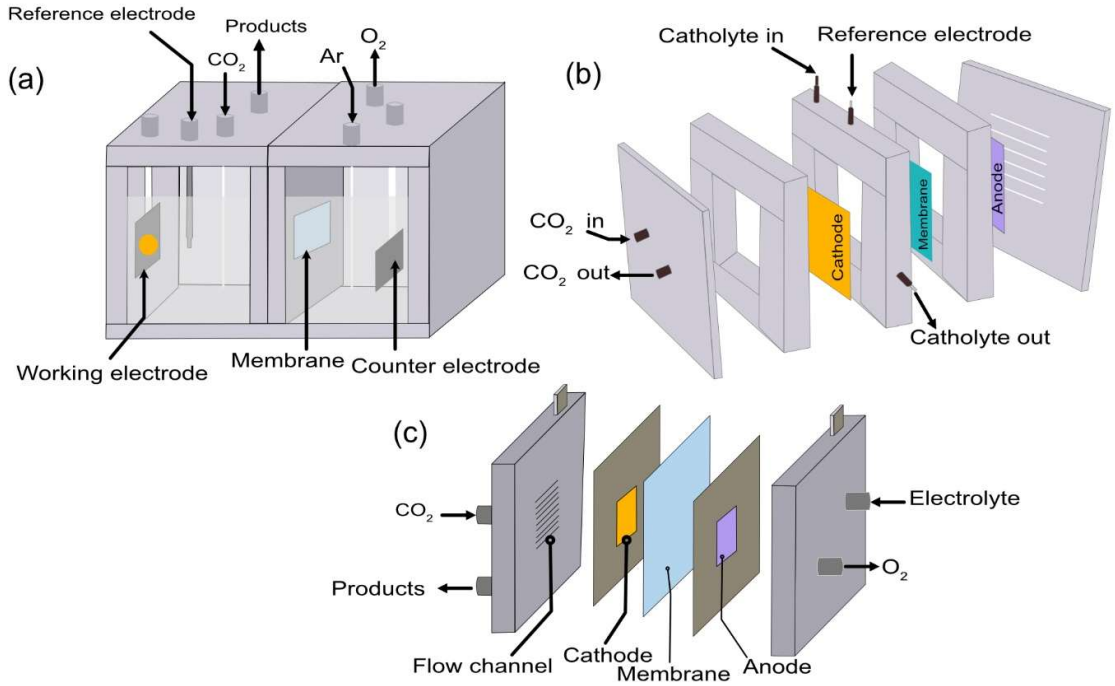

Figure 2.4: Types of cell configurations in CO_2 electroreduction: (a) a H-cell, (b) a liquid flow cell, (c) a zero-gap electrolyzer.

2.7 Electrocatalyst materials for CO_2 electroreduction

The pursuit of efficient CO_2 electroreduction electrocatalysts has led to the exploration of a wide variety of materials, each displaying distinct product selectivity determined by their electronic structure and the binding strength of reaction intermediates (Figure 2.5). Among monometallic catalysts, gold and silver predominantly produce carbon monoxide (CO), owing to their ability to stabilize the *COOH intermediate while allowing easy CO desorption, making them well-suited for two-electron CO_2-to-CO conversion. In contrast, zinc and tin favor the formation of formate ($HCOO^-$) via a two-electron pathway involving *OCHO intermediates, while largely suppressing further reduction. Meanwhile, platinum and nickel bind CO too strongly, which leads to surface poisoning and promotes hydrogen evolution over CO_2 electroreduction. These trends across the periodic table can be understood using d-band theory and the relative binding energies of key intermediates. Metals that bind CO too weakly tend to release it before further reduction can occur, whereas those that bind it too strongly are unable to sustain catalytic turnover. Copper stands out as a unique case, being the only

monometallic catalyst capable of reducing CO_2 beyond CO to form multi-carbon products. This behavior arises from its intermediate *CO binding strength, which enables both sequential hydrogenation and C-C coupling steps that are not accessible on other metals.[32,33,34]

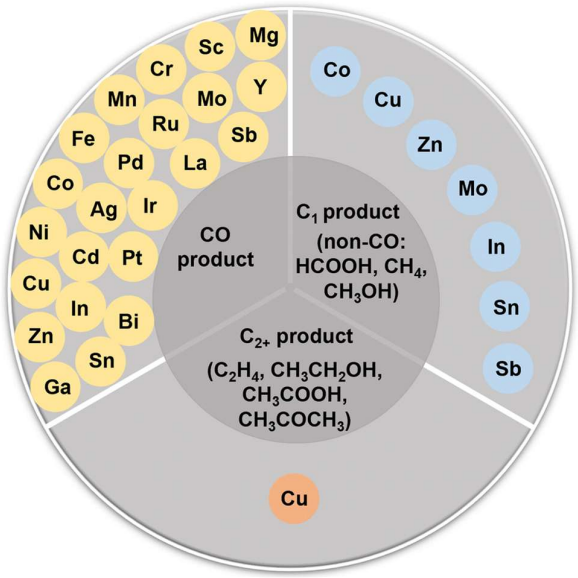

Figure 2.5: Schematic of metals and their CO_2 electroreduction products taken from reference [35]

2.7.1 Copper-based electrocatalysts

The development of efficient electrocatalysts for CO_2 electroreduction has attracted significant attention over the past decades, leading to the investigation of a wide range of materials, including metals, metal oxides, chalcogenides, metal-free materials, and organic electrocatalyst.[36,37] Among these, Copper is the only monometallic electrocatalyst known to catalyze the formation of multi-carbon (C_{2+}) products, such as ethylene, ethanol, and n-propanol, during CO_2 electroreduction. This distinctive behavior is commonly attributed to copper's intermediate binding strength toward key reaction intermediates, which enables C-C coupling while avoiding excessive hydrogen evolution. As a result, copper-based catalysts have become central to research efforts aimed at producing value-added multicarbon fuels and chemicals from CO_2.[38,33]

2.7.2 Nanostructured copper

Nanostructured copper has been widely explored as a strategy to enhance its catalytic performance. Compared to bulk copper, copper nanoparticles (Cu NPs) offer a higher surface-to-volume ratio and expose a greater density of low-coordinated surface sites, which can

influence activity and selectivity.[39] Additionally, particle size, shape, composition, and interparticle distance can be independently tuned to rationally modify catalytic behavior.

Particle size has been shown to play a particularly important role in determining product selectivity. Size-dependent studies on Cu nanoparticles have demonstrated that decreasing the particle diameter from approximately 15 nm to 2 nm leads to increased catalytic activity and enhanced selectivity toward CO and H_2.[40] This behavior has been attributed to the increased abundance of low-coordinated sites on smaller nanoparticles and weaker binding of key intermediates such as *COOH, which favors two-electron reduction pathways over hydrocarbon formation.

Furthermore, the spatial arrangement of Cu nanoparticles on a support has been shown to strongly affect CO_2 reduction selectivity. As the interparticle distance decreases, densely packed Cu NP ensembles with narrow size distributions exhibit increased selectivity toward methane and ethylene. This behavior has been linked to changes in the local reaction environment, including enhanced reactant diffusion, re-adsorption of reaction intermediates, proton depletion, and elevated local interfacial pH. Together, these effects promote C-C coupling and favor the formation of C_2-C_3 hydrocarbons and oxygenates.[41]

Under reaction conditions, densely packed Cu nanoparticles can also undergo structural reconstruction, forming electrocatalytically active cube-like morphologies that further enhance selectivity toward ethylene, ethanol, and n-propanol.[42] These observations highlight the dynamic nature of copper-based catalysts during CO_2 electroreduction and the strong coupling between catalyst structure and reaction environment.

Despite this progress, the overall product selectivity and efficiency of Cu-based catalysts remain limited, and precise control over product distribution remains a major challenge. These limitations motivate continued efforts to tailor the electronic and geometric properties of copper catalysts to improve activity, selectivity, and stability through strategies such as compositional modification and alloying.

2.7.3 Bimetallic electrocatalysts

The challenges associated with pure copper catalysts such as broad product distributions and lack of stability due to susceptibility to surface restructuring have motivated extensive research into alloy electrocatalysts as a strategy for improving CO_2RR performance. Alloys are a combination of metals with one or more elements primarily to achieve improved catalytic properties from their constituent metals. Alloy catalysts for electrochemical reactions are

derived from a wide range of elemental combinations across the periodic table, with transition metals commonly serving as host matrices due to their tunable electronic structure and catalytic activity.[43] These host metals are frequently modified through incorporation of post-transition elements, metalloids, or interstitial species, enabling systematic control of lattice strain, electronic states, and surface adsorption energetics that are critical for electrocatalytic performance.

To leverage on the ability of Cu to form C-C coupling, alloying Cu with different metals enables synergistic interactions between the elements that modify their electronic and geometric structure. Consequently, this modulates CO_2 electroreduction pathways by suppressing competing hydrogen evolution through altered proton adsorption kinetics, stabilizing key reaction intermediates (e.g., CO) via optimized binding strengths, and generating distinct active sites that lower the energy barriers associated with C-C coupling steps.[44]

Bimetallic catalysts can be synthesized by a variety of methods including co-precipitation, electrodeposition, chemical vapor deposition, solgel method, mechanical alloying, and atomic layer deposition techniques. Experimental evidence from bimetallic systems demonstrates clearly that alloying benefits described above can be used to tune CO_2RR selectivity. This was reported by Reske *et al.* for Cu overlayers on Pt, where it was shown that under tensile strain, the formation of CH_4 increased with increasing film thickness.[45] Complementary evidence was provided by Clark *et al.*, who reported a Cu enriched CuAg bimetallic alloys with the incorporation of Ag causing a compressive strain, a shift of the *d*-band center and electronic reconfiguration of the neighboring Cu atoms. These prevented H and O from binding to CO atoms on the Cu surface, limiting the generation of H_2 and subsequent CO reactions, and enhancing the selectivity of CO-derived products.[46]

To show that selectivity of bimetallic catalysts depends on their composition, Kim *et al.* reported a AuCu bimetallic catalyst with increased CO production for every increase in Au concentration. Au_3Cu composition showed the best performance with mass activity in excess of 200 Ag^{-1} at -0.73 V vs RHE.[47] Due to the similarities between pure Au and Au3Cu, it was not possible to attribute the unique CO selectivity only to changes in the electronic structure. Instead, synergetic electrical and geometric effects was proposed to comprehend the AuCu NPs' increased activity for CO_2RR through the adjustment of the intermediate binding strength. Similar results were reported by Li *et al*. for PdCu bimetallic catalyst with Pd7Cu3 showing

the optimal result at -0.8 V vs RHE, with CO faradaic efficiency exceeding 80 %. Theoretically, DFT calculations attributed the increased CO selectivity to the combined geometric and electronic effects in PdCu bimetallic alloy, with Pd atoms being the reactive centers that promote COOH adsorption and CO desorption ability.[48]

However, achieving these benefits without introducing undesirable ensemble effects due to aggregation or extended surface domains of the secondary metal require precise control over alloy composition, atomic distribution, and nanoparticle synthesis. At higher loadings, secondary metal atoms tend to segregate into clusters or surface islands that introduce their own catalytic behavior, complicating mechanistic interpretation and potentially suppressing the C-C coupling activity of Cu.[49] This critical dependence on atomic-scale structure motivates the study of dilute alloy electrocatalysts.

2.8 Dilute alloy electrocatalysts

Dilute alloys are catalysts in which a minor amount of a secondary element is introduced into a host metal, maintaining the host-dominated lattice while locally modifying electronic and geometric properties (Figure 2.6).[43] Such systems are of significant interest because they enable enhanced catalytic activity and selectivity while reducing reliance on precious metals. Unlike conventional bimetallic alloys where secondary metal atoms may aggregate into extended surface domains, dilute alloys may maintain isolated dopant atoms or small agglomerates surrounded by host metal atoms. This ensures preservation of the host metal geometry and maximizes atom efficiency of the dopant metal, which is an important practical consideration when dealing with a precious or scarce material.

A limiting case of dilute alloys is the single atom alloys (SAA), where the secondary element is present at very low surface concentrations such that each dopant atom is entirely surrounded by host metal atoms with no dopant nearest-neighbor contacts. This represents the most structurally precise realization of the dilute alloy concept.[50] As opposed to metal nanoparticles, single atom alloys maximize the atomic efficiency of the secondary atoms, and give well-defined catalytic sites. Additionally, the SAAs are very active in several processes where the corresponding monometallic catalysts are inactive due to the considerably altered adsorption characteristics.[51] Combining these advantages is one of the most promising ways to further enhance electrocatalytic performance and acquire structure-activity relationships in certain coordination environments. This makes a compelling case for single-atom alloys as the rational choice for design of selective CO_2RR electrocatalysts.

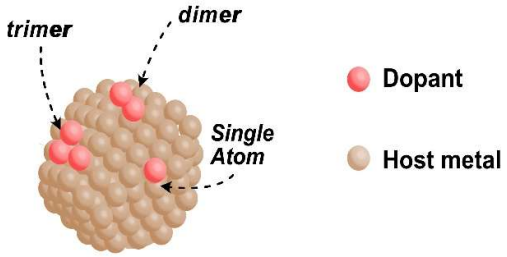

Figure 2.6: Schematic of a dilute alloy.

2.9 Stability considerations in Cu-based dilute alloys: the Cu-Pd model system

One of the key benefits of atomic dispersion of secondary metal within the Cu host is introducing electronic and geometric effects that modify the Cu ensemble and preserve the Cu dominated surface geometry required for the formation of C_{2+} products.[38] Maintaining this atomic dispersion under electrochemical operating conditions, however, represents a critical practical challenge. Under the reducing potentials and high current densities of zero-gap electrolysers, dilute alloy nanoparticles are susceptible to restructuring including dopant surface segregation, electrochemical dissolution, and particle agglomeration, all of which disrupt the electronic modification of Cu active sites and degrade C_{2+} selectivity over time.[52,41] The severity of these pathways depends on the thermodynamics of alloy formation and the synthesis route used, both of which govern the initial atomic distribution of the dopant and its resistance to restructuring under reaction conditions.

Palladium is a particularly well-motivated secondary metal choice for addressing these problems. Cu and Pd are fully miscible across the entire composition range with a negative enthalpy of mixing, thermodynamically favoring stable solid solution formation and resisting phase separation.[53,54] The minor lattice mismatch between Pd and Cu results in a compressive strain in the surrounding Cu lattice that weakens *CO binding on neighboring Cu sites toward the optimal range for C-C coupling.[55] Experimentally, Pd incorporation in Cu-based catalysts has been shown to promote *COOH adsorption and facilitate CO desorption, enhancing CO_2RR selectivity toward C_{2+} products , while atomically dispersed Pd sites have demonstrated a tandem catalytic function promoting two-electron CO_2 to CO conversion at isolated Pd sites while the surrounding Cu ensemble drives further C-C coupling to C_{2+} products.[56] Despite these findings, how Pd content in the strictly dilute region affects catalyst structure, stability, and C_{2+} selectivity retention under industrially relevant conditions remains poorly understood.

3. Methodology

3.1 Chemical and materials

Trioctylamine (98 %), Tetradecylphosphonic acid (98 %), Copper(I) acetate (97 %), Palladium (II) acetate (≥ 98 %), Cesium bicarbonate (99.9 %), Hexane (≥99 %) were purchased from Sigma Aldrich. Carbon paper gas diffusion layer (GDL, Sigracet 39BB) and PiperION® dispersion (5 wt%) were purchased from the Fuel Cell Store. MilliQ water (18.2 MU cm) was obtained from a Millipore system.

3.2 Synthesis of monometallic Cu

Copper nanoparticles were prepared by solvothermal decomposition of Copper(I)acetate (CuOAc) in Trioctylamine (TOA) in the presence of Tetradecyl phosphonic acid (TDPA) and Ascorbic acid (AA) (Figure 3.1).

In a typical synthesis, TOA (10 mL) was heated at 130 °C inside a 25 ml three-neck flask for 30 minutes under a flow of N_2 to remove water and dissolve O_2.

After cooling down to 50 °C, 60 mg of AA dissolved in 0.5 ml of ethylene glycol was transferred to the flask under vigorous stirring. Thereafter, 120 mg of CuOAc and 140 mg TDPA were added with vigorous stirring. The solution was rapidly heated to 180 °C, maintained there for 30 min, rapidly heated to 270 °C, and then held there for an additional 30 min.

Subsequently, the heat source was removed, and the solution was cooled to 100 °C Ethanol was added and the solution mixture was centrifuged at 8000 rpm for 10 minutes. Separated nanoparticles were washed more with hexane and excess ethanol mixtures and finally redispersed in hexane for further use and characterization.

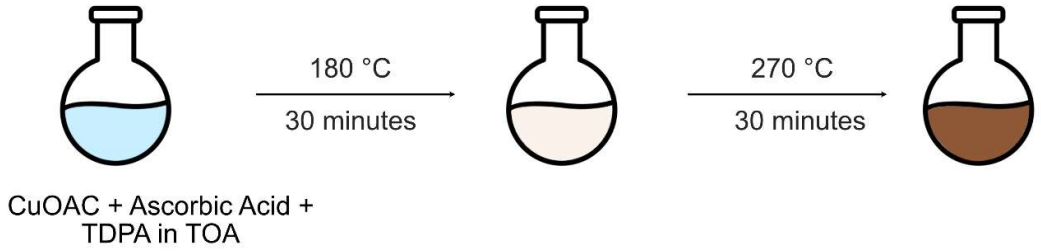

Figure 3.1: Schematic of the solvothermal synthesis of Cu nanoparticles used in this work.

3.3 Synthesis of CuPd alloy nanoparticles via sequential and co-reduction

For the synthesis of CuPd alloy nanoparticles via sequential reduction, monometallic Cu nanoparticles were first prepared following the procedure described in Section 3.2. After

heating the reaction mixture to 270 °C and maintaining it for 30 minutes, the solution was cooled to 200 °C. A predetermined amount of $Pd(OAc)_2$ dissolved in 0.5 mL oleylamine was then added dropwise, and the reaction was maintained at this temperature for an additional 30 minutes (Figure 3.2).

Subsequently, the heat source was removed, and the reaction mixture was cooled to 100 °C. Ethanol was added to precipitate the nanoparticles, followed by centrifugation at 8000 rpm for 10 minutes. The collected nanoparticles were washed multiple times using a hexane-ethanol mixture and finally redispersed in hexane for further use and characterization.

For the co-reduction approach, Cu and Pd precursors were introduced simultaneously and reduced using the same protocol described for the synthesis of monometallic Cu nanoparticles in the previous section (Figure 3.2).

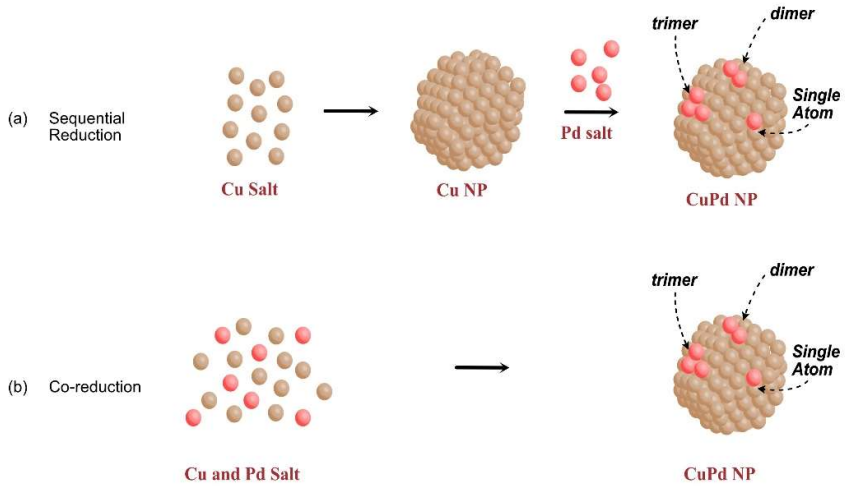

Figure 3.2: Schematic of the synthesis of CuPd dilute alloys via sequential and coreduction methods.

3.4 Material characterization

3.2.1 Inductively coupled plasma mass spectroscopy

The Cu and Pd contents were determined via inductively coupled plasma mass spectrometry (ICP-MS). The samples were digested in freshly prepared aqua regia ($HCl:HNO_3$, 3:1 v/v). Briefly, 1 mL of the colloidal nanoparticle dispersion in hexane was dried under a nitrogen stream to remove the organic solvent. Subsequently, 2.5 mL of aqua regia was added, and the mixture was kept at room temperature until complete digestion was achieved. The resulting solution was diluted to a final volume of 15 mL with Milli-Q water to obtain the stock solution. Serial dilution was performed by transferring 0.5 mL of the stock solution into 49.5 mL of 0.5

M HNO_3. Finally, 1 mL of this intermediate solution was further diluted with 9 mL of 0.5 M HNO_3 containing 2 ppb yttrium as an internal standard prior to analysis.

3.2.2 X-Ray photoelectron spectroscopy

X-ray photoelectron spectroscopy (XPS) was performed using a HI5000 VersaProbe III instrument equipped with a monochromatic Al Kα source. Dual charge compensation was applied during data acquisition. All spectra were calibrated with respect to the adventitious carbon C 1s peak at 284.5 eV.

XPS analysis was conducted to determine the surface chemical composition and oxidation states of Cu and CuPd alloy nanoparticles. Colloidal dispersions of the nanoparticles in hexane were drop-casted onto silicon wafers and allowed to dry under ambient conditions. Measurements were carried out without further sample preparation.

3.2.3 Transmission electron microscopy

Transmission electron microscopy (TEM) was employed to investigate the morphology and size distribution of the synthesized nanoparticles. TEM is a high-resolution imaging technique in which a thin sample is irradiated with a high-energy electron beam, and the transmitted electrons are used to form an image with nanometer-scale resolution. In this thesis, imaging was carried out using an FEI Titan 80–300 microscope operated in TEM mode at an accelerating voltage of 200 kV. Particle size distributions were analyzed using the Fiji (ImageJ) image analysis software. TEM samples were prepared by drop-casting a diluted nanoparticle suspension onto a Cu grid, followed by solvent evaporation under ambient conditions.

High-angle annular dark-field scanning transmission electron microscopy (HAADF-STEM) was performed using a JEOL ARM200F monochromated microscope equipped with a Schottky field emission gun, a double Wien monochromator, and both probe and image aberration correctors. The instrument was further equipped with dual silicon drift detectors (SDDs) for energy-dispersive X-ray spectroscopy (EDS), enabling elemental mapping and compositional analysis at high spatial resolution.

Samples were prepared by drop-casting a diluted nanoparticle dispersion onto silicon nitride TEM grids (2.9 mm hexagonal grids with eight 100 × 100 µm windows and one 100 × 350 µm window) and allowing the solvent to evaporate under ambient conditions. Prior to use, the grids were cleaned using a suspension of activated carbon in ethanol to minimize contamination from surface ligands during electron microscopy analysis.

3.3 Electrode preparation

A catalyst ink was prepared by dispersing the desired amount of catalyst in an isopropanol–water mixture (0.9:0.1, v/v) together with a PiperION ionomer dispersion (5 wt%) as the binder. For each milligram of catalyst, 26.7 µL of solvent and 20 µL of ionomer dispersion were used, corresponding to a catalyst-to-ionomer weight ratio of 9:1. The mixture was homogenized by ultrasonication in a water bath (T < 35 °C) for 30 minutes to obtain a uniform dispersion.

The catalyst ink was deposited onto the microporous layer (MPL) side of a commercially available gas diffusion layer (Sigracet 39BB) using a hand-brushing method. During deposition, the GDL was placed on a hot plate maintained at 60 °C to promote rapid solvent evaporation and ensure uniform coating. The catalyst loading was controlled at 1 mg cm^{-2} by adjusting the ink volume and verified gravimetrically before and after deposition. The obtained Gas Diffusion Electrode (GDE) serve as the cathode.

3.4 Electrochemical measurements

Electrochemical measurements were performed in a zero-gap configuration (Figure 3.3) having a two-electrode configuration using a Biologic-VSP potentiostat.

A 40 µm thick PiperION anion-exchange membrane (AEM) was employed the membrane, IrO_2 supported on Ti felt as the anode and 0.1 M $CsHCO_3$ as the anolyte. The CO_2 feed (99.996%, Nippon Gases) and anolyte flow rates were both maintained at 20 mL min^{-1}. Electrolysis experiments were conducted for 15 minutes at current densities of 100 mA cm^{-2}, 200 mA cm^{-2}, and 300 mA cm^{-2} in sequence, with fresh anolyte supplied for each current density. All measurements were performed in duplicate to ensure reproducibility and enable estimation of standard deviations.

Gaseous products were analyzed using a Perkin Elmer Clarus 590 GC equipped with a thermal conductivity detector and flame ionization detector. The CO_2 gas flow rate was controlled by a red-y smart series thermal mass flow controller from Vögtlin instruments. The CO_2 gas is N45 purchased from Air Liquide. Liquid products formed at the cathode were quantified using an Agilent 1260 Infinity II HPLC equipped with Refractive Index Detector (RID). The anolyte was also collected and analyzed by HPLC after each experiment to assess product crossover.

The Faradaic efficiency (FE) for each product was calculated according to:

$$FE_i = \frac{n \cdot F \cdot Ci \cdot V}{I}$$

where n is the number of electrons transferred, F is Faraday's constant, C_i is the molar concentration of product i, V is the volumetric flow rate, and I is the applied current using chronopotentiometry.

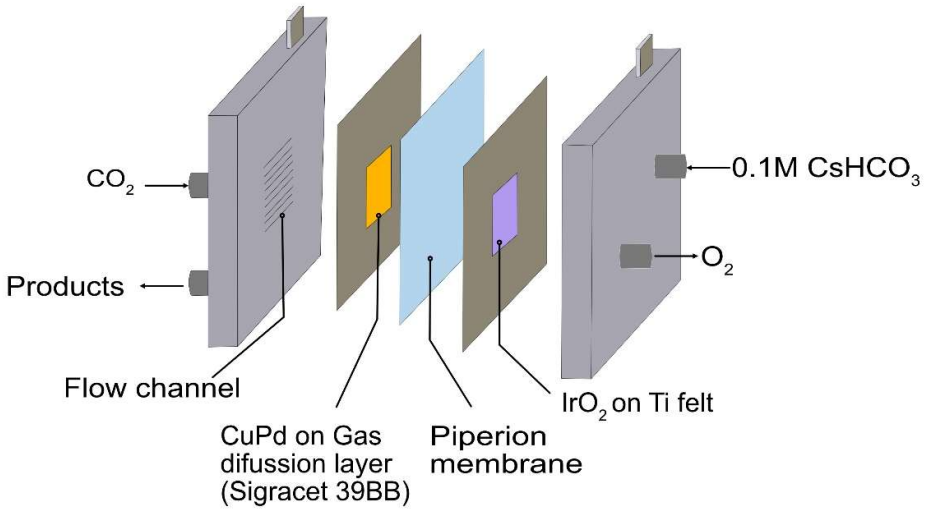

Figure 3.3: Schematic diagram of the zero-gap electrolyzer and components used in thiswork.

4. Summary of appended papers

This thesis is based on two complementary studies investigating how Pd composition (Paper I) and synthesis route (Paper II) govern the structure and CO_2 electroreduction performance of Cu-Pd dilute alloy nanoparticles in a zero-gap electrolyzer at industrially relevant current densities.

Paper I

Paper I examines the effect of Pd composition across the dilute alloy regime (2-6 at. %) on CO_2RR performance. A series of Cu-Pd dilute alloy nanoparticles with nominal Pd compositions of 2, 4.5, and 6 at.% were synthesized by a solvothermal method and characterized to confirm composition, morphology, and oxidation state. ICP-MS analysis confirmed that the measured bulk Pd compositions were close to the nominal targets at 1.71, 4.69, and 6.33 at. % respectively, demonstrating good synthetic control over alloy composition across the dilute regime. TEM imaging (Figure 4.1) revealed that all samples consisted of well-dispersed nanoparticles with a narrow size distribution of 5-6 nm, with no significant difference in particle size or morphology between Cu and Cu-Pd. XPS analysis confirmed that both Cu and Pd were present in the metallic state at the nanoparticle surface prior to electrochemical testing, consistent with successful reduction of both metal precursors and the minor surface oxide layers due to air exposure, that could mask the intrinsic catalytic behavior of the alloy.

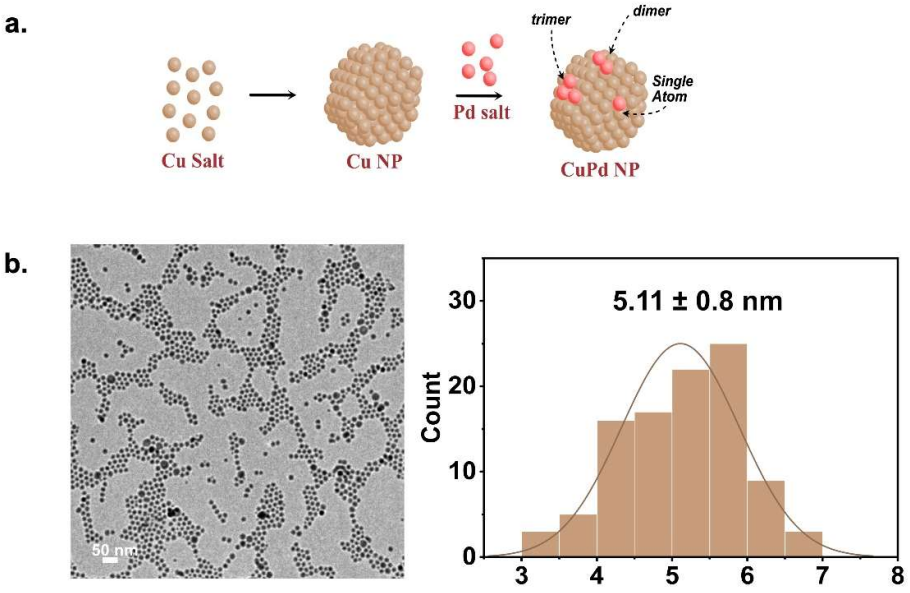

Figure 4.1: (a) Schematic of CuPd synthesis; (b) TEM image of $Cu_{95.5}Pd_{4.5}$ and its size distribution.

Electrochemical performance was evaluated in a zero-gap electrolyzer at current densities of 100, 200, and 300 mA cm^{-2}, with gaseous products analyzed by online gas chromatography and liquid products quantified by HPLC. The results reveal three distinct performance regimes, each governed by a different balance between ensemble disruption and structural stabilization (Figure 4.2). At 100 mA cm^{-2}, monometallic Cu outperforms all Cu-Pd compositions with a C_{2+} Faradaic efficiency of 40.25 %, a C_{2+}/C_1 ratio of 2.8, and an H_2 FE of 16 % as Pd incorporation blocks the Cu active sites required for C-C coupling and shifts selectivity toward C_1 products. At higher current densities, however, this trend reverses: pure Cu exhibits a sharp doubling in H_2 evolution from 16 % to 35 %, accompanied by a drop in C_{2+} FE from 40.25 % to 29 % between 100 and 200 mA cm^{-2}, while Cu-Pd dilute alloys suppress this current-density-dependent HER surge and improve faradaic efficiency toward CO_2 reduction products. $Cu_{95.5}Pd_{4.5}$ maintains an H_2 FE of 26 % (barely unchanged from 100 mA cm^{-2}), C_{2+} FE of 35 %, and C_{2+}/C_1 ratio of 3.20 outperforming pure Cu under identical conditions. An optimal Pd content of 2-4.5 at. % is identified, beyond which excessive dilution of Cu active sites diminishes performance. These results establish that dilute Pd alloying functions as a HER suppressor under high-rate operating conditions and provide a compositional design principle for robust Cu-based catalysts in practical zero-gap CO_2 electrolyzers.

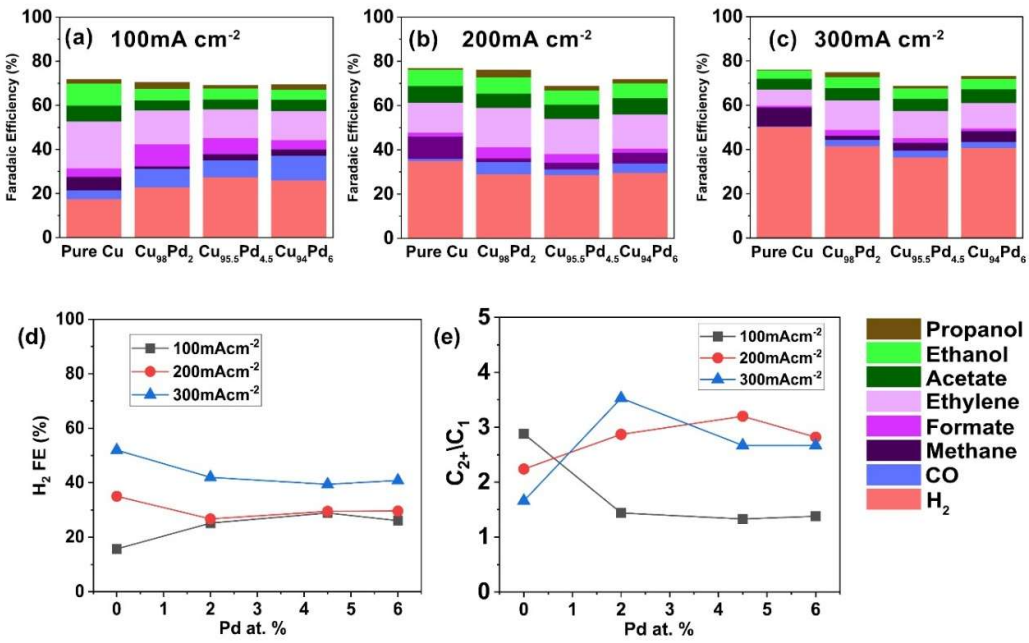

Figure 4.2: (a) Full product distribution at 100 $mAcm^{-2}$; (b) at 200 $mAcm^{-2}$; (c) at 300 $mAcm^{-2}$ (d) H_2 Faradaic Efficiency; (e) ratio of total C_{2+} to total C_1 Faradaic efficiency.

Paper II

While Paper I established that dilute Pd alloying suppresses current-density-dependent hydrogen evolution and preserves C_{2+} selectivity in Cu-based catalysts, it evaluated catalysts prepared by a single synthesis route. A fundamental but underexplored question remains on how the synthesis route and the atomic-scale Pd distribution it produces independently govern catalytic performance for fixed bulk composition. In bimetallic nanoparticle systems, the same nominal composition prepared by different routes can produce different atomic-scale structures, with different degrees of dopant surface enrichment or depletion and different probabilities of dopant nearest-neighbor contacts. Paper II addresses these by systematically comparing Cu-Pd nanoparticles prepared by sequential reduction and co-reduction across four Pd compositions as shown in Figure 3.2. Sequential reduction, in which Cu nanoparticles are formed first and Pd subsequently incorporated, appears to produce preferentially isolated surface Pd sites through a core-enriched Pd distribution, while co-reduction appears to produce a more homogeneous Pd distribution with higher surface Pd density at equivalent bulk composition, as confirmed by STEM-EDS characterization (Figure 4.3).

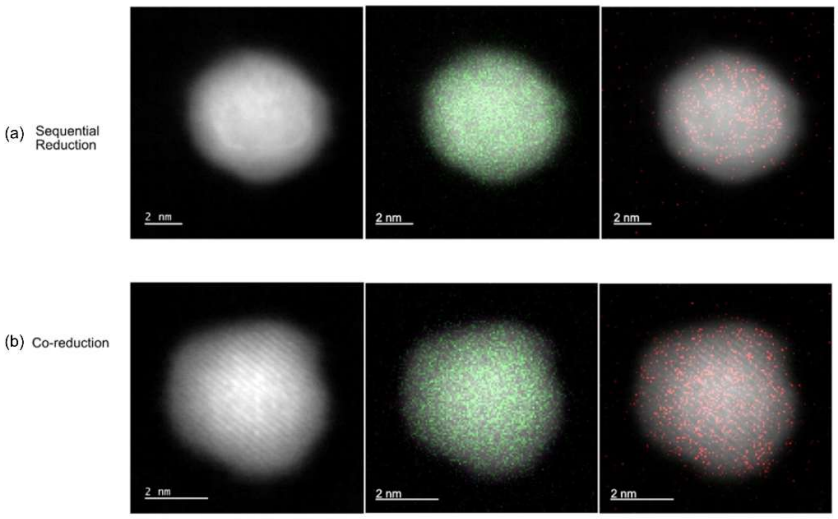

Figure 4.3: STEM-EDS images of Cu-Pd nanoparticles synthesized by (a) sequential reduction (4.5 at. % Pd) and; (b) co-reduction (6 at. % Pd).

Electrochemical performance was evaluated in a zero-gap electrolyzer at 200 mA cm^{-2} which was established as the current density identified in Paper I as the onset of significant performance divergence between Cu and Cu-Pd. At low Pd compositions, sequentially reduced samples consistently outperform their co-reduced counterparts prepared at identical bulk composition (Figure 4.4). The difference is most clearly illustrated at nominal composition 4.5

at.% Pd, where the sequentially reduced alloys achieve a C_{2+} FE of 31%, compared to 23% for the co-reduced equivalent which may be attributed to the difference in Pd spatial distribution between the two synthesis routes (Figure 4.4). At higher Pd compositions, the performance gap between the two routes narrows, consistent with the increasing probability that Pd distribution in both synthesis are similar.

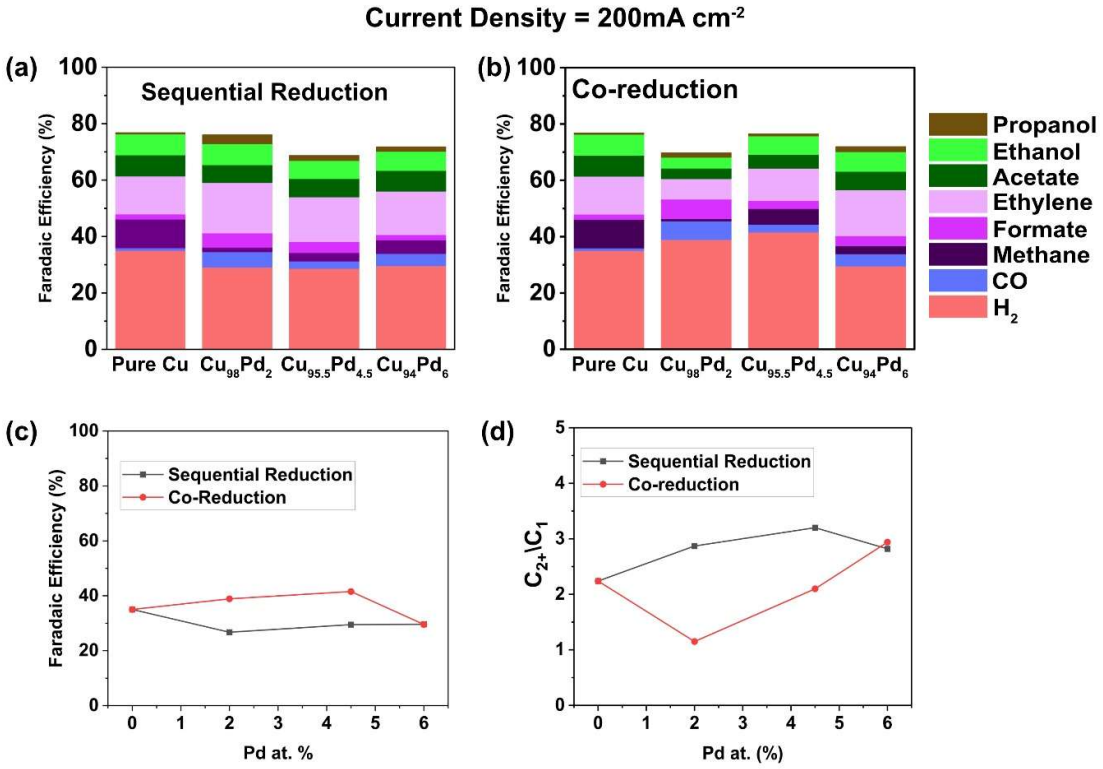

Figure 4.4: Full product distribution for (a) Sequential Reduction, (b) Co-Reduction, and (c) H_2 Faradaic Efficiency, (d) ratio of total C_{2+} to total C_1 Faradaic efficiency.

Together, these studies from papers I and II establish that both composition and synthesis route must be jointly considered to realize the full performance benefits of the dilute alloy architecture and provide transferable design principles for robust and selective Cu-based CO_2 electroreduction catalysts under practical operating conditions.

5. Conclusion and outlook

This thesis investigated how alloy composition and synthesis pathway jointly govern the structure and electrocatalytic performance of Cu-Pd dilute alloy nanoparticles for CO_2 electroreduction in zero-gap electrolyzers at industrially relevant current densities.

The first study established that the effect of Pd incorporation is strongly current-density dependent. At 100 mA cm^{-2}, Pd is detrimental, blocking the Cu surface sites required for C-C coupling and shifting selectivity toward C_1 products. At 200-300 mA cm^{-2}, the trend reverses: pure Cu exhibits a drastic increase in H_2 FE accompanied by significant C_{2+} selectivity loss, while Cu-Pd dilute alloys suppress this current-density-dependent HER surge and maintain faradaic efficiency toward CO_2 reduction products. An optimal Pd content of 2-4.5 at.% is identified, beyond which active Cu site dilution outweighs stabilization. These results establish dilute Pd as a HER suppressor under high-rate conditions and demonstrate that evaluating bimetallic CO_2RR catalysts at mild current densities alone is insufficient.

The second study established that synthesis route independently governs catalytic performance at fixed bulk composition. Sequential reduction produces preferentially isolated surface Pd sites through core-enriched Pd distribution, while co-reduction yields homogeneous distribution with higher surface Pd density as confirmed by STEM-EDS. At 200 mA cm^{-2}, sequentially reduced Cu-Pd achieves C_{2+} FE of 31% compared to 23% for the co-reduced equivalent, establishing that Pd surface composition is dictated by the synthesis route in the dilute regime.

By and large, these findings show that composition and synthesis routes must be jointly optimized to realize the full performance benefits of the dilute alloy electrocatalysts and provide design principles for robust Cu-based CO_2 electroreduction catalysts under practical operating conditions.

Looking ahead, several directions warrant further investigation, some of which are currently ongoing. DFT calculations of hydrogen adsorption energy and *CO binding strength on Cu sites adjacent to isolated Pd atoms would provide the mechanistic backbone currently missing from the experimental observations. Long-term stability studies under continuous high-current operation would address the open question of whether the Pd stabilization effect persists over extended operation. Finally, tracking how Pd evolves structurally and compositionally under operating conditions using operando characterization techniques would provide direct insight into the dynamic behavior of the dilute alloy architecture during CO_2 electroreduction.

Acknowledgments

This work was carried out at the Department of Chemistry and Chemical Engineering, Competence Centre for Catalysis (KCK), and Chalmers Material Analysis Laboratory (CMAL), Chalmers University of Technology, Gothenburg, Sweden as well as Department of Physics, Technical University of Denmark. Financial support from Area of Advance Energy and FORMAS is gratefully acknowledged.

I would like to express my sincere gratitude to my supervisors, Asst. Prof. Mathilde Luneau and Prof. Magnus Skoglundh, for their unwavering support, scientific guidance, and encouragement throughout this journey, and my examiner, Prof. Anna Martinelli, for evaluating and keeping up with the progress of my studies.

Also, I would also like to thank Prof. Brian Seger and Dr. Mohd Monis Ayyub at the Technical University of Denmark for the fruitful collaboration on the zero-gap electrolyser testing. Their generosity with both equipment and time made a critical part of this work possible.

The Swedish Research Council and Swedish Foundation for Strategic Research are acknowledged for access to ARTEMI, the Swedish National Infrastructure in Advanced Electron Microscopy (2021-00171 and RIF21-0026).

Further, I am also grateful to Dr. Mustapha Saleh and Esraa Darwish for assistance with ICP-MS measurements, the ARTEMI support staffs, Dr. Andrew Yankovich and Dr. Lunjie Zeng, Dr. Michael Wilms for XPS characterization and my colleagues at Luneau Lab and division of applied chemistry for creating an excellent working environment.

Finally, I am deeply grateful to my family, especially my wife, Fatima, and our children, whose love, patience, and daily presence have been my greatest source of strength. This work is as much yours as it is mine.

References

1. Trenberth, K. E. Climate change caused by human activities is happening and it already has major consequences. *J. Energy Nat. Resour. Law* **36**, 463–481 (2018).
2. Lelieveld, J., Haines, A., Burnett, R., Tonne, C., Klingmuller, K., Munzel, T., & Pozzer, A. Air pollution deaths attributable to fossil fuels: observational and modelling study. (2023)
3. Perera, F. P. Multiple Threats to Child Health from Fossil Fuel Combustion: Impacts of Air Pollution and Climate Change. *Environ. Health Perspect.* **125**, 141–148 (2017).
4. Barbir, F., Veziroğlu, T. N. & Plass, H. J. Environmental damage due to fossil fuels use. *Int. J. Hydrog. Energy* **15**, 739–749 (1990).
5. San-Akca, B., Sever, S. D. & Yilmaz, S. Does natural gas fuel civil war? Rethinking energy security, international relations, and fossil-fuel conflict. *Energy Res. Soc. Sci.* **70**, 101690 (2020).
6. Barthelmie, R. J., Pryor, S. C., Barthelmie, R. J. & Pryor, S. C. Climate Change Mitigation Potential of Wind Energy. *Climate* **9**, (2021).
7. Kabir, E., Kumar, P., Kumar, S., Adelodun, A. A. & Kim, K.-H. Solar energy: Potential and future prospects. *Renew. Sustain. Energy Rev.* **82**, 894–900 (2018).
8. Melero, J. A., Iglesias, J. & Garcia, A. Biomass as renewable feedstock in standard refinery units. Feasibility, opportunities and challenges. *Energy Environ. Sci.* **5**, 7393–7420 (2012).
9. Wang, G., Chen, G., Ding, Y., Cai, P., Yi, L., Li, Y., Tu, C., Hou, Y., Wen, Z. & Dai, L. Electrocatalysis for CO_2 conversion: from fundamentals to value-added products. *Chem. Soc. Rev.* **50**, 4993–5061 (2021).
10. Liu, L., Akhoundzadeh, H., Li, M. & Huang, H. Alloy Catalysts for Electrocatalytic CO_2 Reduction. *Small Methods* 2300482 (2023)

11. O'Mullane, A. P. Electrochemistry. in *Reference Module in Chemistry, Molecular Sciences and Chemical Engineering*; Elsevier, 2013.
12. Allen J. Bard and Larry R. Faulkner, Electrochemical Methods: Fundamentals and Applications, New York: Wiley, 2001, 2nd ed. *Russ. J. Electrochem.* **38**, 1364–1365 (2002).
13. An Idea to Explore: Understanding Redox Reactions in Biochemistry. https://iubmb.onlinelibrary.wiley.com/doi/epdf/10.1002/bmb.21189
14. Atkins, P. W. & Jones, L. *Chemical Principles: The Quest for Insight*. (W.H. Freeman, 2010).
15. Newman, J. & Thomas-Alyea, K. E. *Electrochemical Systems*. (John Wiley & Sons, 2004).
16. Kortlever, R., Shen, J., Schouten, K. J. P., Calle-Vallejo, F. & Koper, M. T. M. Catalysts and Reaction Pathways for the Electrochemical Reduction of Carbon Dioxide. *J. Phys. Chem. Lett.* **6**, 4073–4082 (2015).
17. Dickinson, E. J. F. & Wain, A. J. The Butler-Volmer equation in electrochemical theory: Origins, value, and practical application. *J. Electroanal. Chem.* **872**, 114145 (2020).
18. Fuller, T. F.; Harb, J. N. *Electrochemical Engineering*; Wiley: Hoboken, NJ, 2018
19. Weiss, R. F. Carbon dioxide in water and seawater: the solubility of a non-ideal gas. *Mar. Chem.* **2**, 203–215 (1974).
20. Weng, L.-C., Bell, A. T. & Weber, A. Z. Modeling gas-diffusion electrodes for CO_2 reduction. *Phys. Chem. Chem. Phys.* **20**, 16973–16984 (2018).
21. Jeanty, P., Scherer, C., Magori, E., Weisner-Fleischer, K., Hinrichsen, O., & Fleischer, M. Upscaling and continuous operation of electrochemical CO_2 to CO conversion in aqueous solutions on silver gas diffusion electrodes. *J. CO2 Util.* **24**, 454–462 (2018).

22. Dev, A., Srivastava, A. K. & Karmakar, S. New Generation Hybrid Nanobiocatalysts. in *Handbook of Nanomaterials for Industrial Applications* 217–231 (Elsevier, 2018).
23. Ooka, H., Huang, J. & Exner, K. S. The Sabatier Principle in Electrocatalysis: Basics, Limitations, and Extensions. *Front. Energy Res.* **9**, (2021).
24. Li, X., Guan, X., Zhu, L., Li, H., Yin, X., Sun, S., Xu, H., Fan, Y., Li, P., Hu, L., Wu, Z., Pan, H., Wang, X., Cheng, Z., Jia, B., & Ma, T. Electron transfer in catalysis: from fundamentals to strategies. *Chem. Soc. Rev.* **54**, 11423–11467 (2025).
25. Friedlingstein, P. *et al.* Global Carbon Budget 2022. *Earth Syst. Sci. Data* **14**, 4811–4900 (2022).
26. Smith, W. A., Burdyny, T., Vermaas, D. A. & Geerlings, H. Pathways to Industrial-Scale Fuel Out of Thin Air from CO2 Electrolysis. *Joule* **3**, 1822–1834 (2019).
27. Elouarzaki, K., Kannan, V., Jose, V., Sabharwal, H. S. & Lee, J.-M. Recent Trends, Benchmarking, and Challenges of Electrochemical Reduction of CO_2 by Molecular Catalysts. *Adv. Energy Mater.* **9**, 1900090 (2019).
28. Kortlever, R., Shen, J., Schouten, K. J. P., Calle-Vallejo, F. & Koper, M. T. M. Catalysts and Reaction Pathways for the Electrochemical Reduction of Carbon Dioxide. *J. Phys. Chem. Lett.* **6**, 4073–4082 (2015).
29. Zhu, D. D., Liu, J. L. & Qiao, S. Z. Recent Advances in Inorganic Heterogeneous Electrocatalysts for Reduction of Carbon Dioxide. *Adv. Mater.* **28**, 3423–3452 (2016).
30. Zhang, L., Zhao, Z.-J. & Gong, J. Nanostructured Materials for Heterogeneous Electrocatalytic CO_2 Reduction and their Related Reaction Mechanisms. *Angew. Chem. Int. Ed.* **56**, 11326–11353 (2017).
31. Wang, G., Chen, G., Ding, Y., Cai, P., Yi, L., Li, Y., Tu, C., Hou, Y., Wen, Z. & Dai, L. Electrocatalysis for CO_2 conversion: from fundamentals to value-added products. *Chem. Soc. Rev.* **50**, 4993–5061 (2021).

32. Zhu, W., Michalsky, R., Metin, Ö., Lv, H., Guo, S., Wright, C., Sun, X., Peterson, A. A., & Sun, S. Monodisperse Au Nanoparticles for Selective Electrocatalytic Reduction of CO_2 to CO. *J. Am. Chem. Soc.* **135**, 16833–16836 (2013).

33. Hori, Y., Wakebe, H., Tsukamoto, T. & Koga, O. Electrocatalytic process of CO selectivity in electrochemical reduction of CO_2 at metal electrodes in aqueous media. *Electrochimica Acta* **39**, 1833–1839 (1994).

34. da Silva Freitas, W., D'Epifanio, A. & Mecheri, B. Electrocatalytic CO_2 reduction on nanostructured metal-based materials: Challenges and constraints for a sustainable pathway to decarbonization. *J. CO_2 Util.* **50**, 101579 (2021).

35. Chen, C., Li, J., Tan, X., Zhang, Y., Li, Y., He, C., Xu, Z., Zhang, C., & Chen, C. Harnessing single-atom catalysts for CO_2 electroreduction: a review of recent advances. *EES Catal.* **2**, 71–93 (2024).

36. She, X., Wang, Y., Xu, H., Chi Edman Tsang, S. & Ping Lau, S. Challenges and Opportunities in Electrocatalytic CO_2 Reduction to Chemicals and Fuels. *Angew. Chem. Int. Ed.* **61**, e202211396 (2022).

37. Jhong, H.-R. "Molly", Ma, S. & Kenis, P. J. Electrochemical conversion of CO_2 to useful chemicals: current status, remaining challenges, and future opportunities. *Curr. Opin. Chem. Eng.* **2**, 191–199 (2013).

38. Peterson, A. A. & Nørskov, J. K. Activity Descriptors for CO_2 Electroreduction to Methane on Transition-Metal Catalysts. *J. Phys. Chem. Lett.* **3**, 251–258 (2012).

39. Loiudice, A., Lobaccaro, P., Kamili, A. E., Thao, T., Huang, H. B., Ager, W. J., & Bounsanti, R. Tailoring Copper Nanocrystals towards C_2 Products in Electrochemical CO_2 Reduction. *Angew. Chem. Int. Ed.* **55**, 5789–5792 (2016).

40. Reske, R., Mistry, H., Behafarid, F., Cuenya, B. R. & Strasser, P. Particle Size Effects in the Catalytic Electroreduction of CO_2 on Cu Nanoparticles. *J. Am. Chem. Soc.* **136**, 6978–6986 (2014).
41. Auer, A., Andersen, M., Wernig, E., Hörmann, N. G., Buller, N., Reuter, K., & Kunze-Liebhäuser, J. Self-activation of copper electrodes during CO electro-oxidation in alkaline electrolyte. *Nat. Catal.* **3**, 797–803 (2020).
42. Grosse, P., Yoon, A., Rettenmaier, C., Herzog, A., Chee, S. W., & Cuenya, B. C.. Dynamic transformation of cubic copper catalysts during CO_2 electroreduction and its impact on catalytic selectivity. *Nat. Commun.* **12**, 6736 (2021).
43. Du, M., Li, X., Pang, H. & Xu, Q. Alloy electrocatalysts. *EnergyChem* **5**, 100083 (2023).
44. Bagger, A., Ju, W., Varela, A. S., Strasser, P. & Rossmeisl, J. Electrochemical CO_2 Reduction: A Classification Problem. *ChemPhysChem* **18**, 3266–3273 (2017).
45. Reske, R., Duca, M., Oezaslan, M., Schouten, K., Koper, M., & Strasser, P. Controlling Catalytic Selectivities during CO_2 Electroreduction on Thin Cu Metal Overlayers. *J. Phys. Chem. Lett.* **4**, 2410–2413 (2013).
46. Clark, E. L., Hahn, C., Jaramillo, T. F. & Bell, A. T. Electrochemical CO_2 Reduction over Compressively Strained CuAg Surface Alloys with Enhanced Multi-Carbon Oxygenate Selectivity. *J. Am. Chem. Soc.* **139**, 15848–15857 (2017).
47. Kim, D., Resasco, D., Yu, Yi., Asiri, A. M., & Yang, P. Synergistic geometric and electronic effects for electrochemical reduction of carbon dioxide using gold–copper bimetallic nanoparticles. *Nat. Commun.* **5**, 4948–4948 (2014).
48. Li, M., Wang, J., Li, P., Chang, K., Li, C., Wang, T., Jiang, B., Zhang, H., Liu, H., Yamuchi, Y., Umezawa, N., & Ye, J. Mesoporous palladium–copper bimetallic electrodes for selective electrocatalytic reduction of aqueous CO_2 to CO. *J. Mater. Chem. A* **4**, 4776–4782 (2016).

49. Bagger, A., Ju, W., Varela, A. S., Strasser, P. & Rossmeisl, J. Electrochemical CO_2 Reduction: A Classification Problem. *ChemPhysChem* **18**, 3266–3273 (2017).
50. Shi, X. *et al.* Metal–support frontier orbital interactions in single-atom catalysis. *Nature* **640**, 668–675 (2025).
51. Wang, Q. *et al.* Lanthanide single-atom catalysts for efficient CO_2-to-CO electroreduction. *Nat. Commun.* **16**, 2985 (2025).
52. Ruban, A. V., Skriver, H. L. & Nørskov, J. K. Surface segregation energies in transition-metal alloys. *Phys. Rev. B* **59**, 15990–16000 (1999).
53. Ishijima, M., Todoroki, N., Cuya Huaman, J. L., Tanaka, Y. & Balachandran, J. Kinetically Controlled Direct Synthesis of B2- and A1-Structured Cu–Pd Nanoparticles. *Inorg. Chem.* **62**, 19270–19278 (2023).
54. Todoroki, N., Ishijima, M., Huaman, J. L. C., Tanaka, Y. & Balachandran, J. Composition sensitive selectivity and activity of electrochemical carbon dioxide reduction on Pd–Cu solid-solution alloy nanoparticles. *Catal. Sci. Technol.* **13**, 5025–5032 (2023).
55. Liu, C. *et al.* Local-strain-induced CO_2 adsorption geometries and electrochemical reduction pathway shift. *Natl. Sci. Rev.* **11**, nwae191 (2024).
56. Huang, H., Tsai, T.-H., Huang, Z.-Y., Tsai, M.-K. & Chou, T.-C. Selective electrochemical reduction of CO_2 to ethanol via atomic-level Pd-incorporated cu alloy catalysts under industrially relevant conditions. *Chem. Eng. J.* **523**, 168675 (2025).